Using small molecules to overcome drug resistance induced by a viral oncogene

Inese Smukste,[1] Oneil Bhalala,[1] Marco Persico,[1] and Brent R. Stockwell[1,*]

[1] Department of Biological Sciences and Department of Chemistry, Columbia University, Fairchild Center, MC 2406, 1212 Amsterdam Avenue, New York, New York 10027
*Correspondence: stockwell@biology.columbia.edu

Summary

We used small molecule screening to discover compounds and mechanisms for overcoming *E6* oncogene-mediated drug resistance. Using high-throughput screening in isogenic cell lines, we identified compounds that potentiate doxorubicin's lethality in E6-expressing colon cancer cells. Such compounds included quaternary ammonium salts, protein synthesis inhibitors, 11-deoxyprostaglandins, and two additional classes of compounds—analogs of 1,3-bis(4-morpholinylmethyl)-2-imidazolidinethione (a thiourea) and acylated secondary amines that we named indoxins. Indoxins upregulated topoisomerase IIα, the target of doxorubicin, thereby increasing doxorubicin lethality. We developed a photolabeling strategy to identify targets of indoxin and discovered a nuclear actin-related protein complex as a candidate indoxin target.

Introduction

The ability of tumor cells to survive treatment with any of numerous unrelated anticancer drugs is known as multidrug resistance (MDR) (Krishna and Mayer, 2000). Specifically, resistance to apoptosis-inducing drugs is one of the hallmarks of cancer (Hanahan and Weinberg, 2000): most cancer cells eventually acquire alterations that enable them to evade apoptosis. This ability contributes to the drug-resistant phenotype found in human cancers (Johnstone et al., 2002). For example, the tumor suppressor protein p53, which is a central signaling protein involved in apoptosis, is mutated in more than 50% of human cancers (Levine, 1997). Most commonly, the *TP53* gene is inactivated via mutation (Hainaut et al., 1998; Olivier et al., 2002). However, amplification of the *Murine Double Minute 2* (*MDM2*) oncogene, which encodes an E3 ubiquitin ligase that targets p53 for proteasomal degradation, also leads to loss of p53 protein (Michael and Oren, 2003). In addition, viral oncoproteins, such as HPV E6, SV40 large T antigen, and human hepatitis B virus X protein, are capable of interfering with p53 function, and thereby increasing the resistance of tumor cells to chemotherapeutic agents (Collot-Teixeira et al., 2004).

HPV type 16 and 18 (HPV16 and HPV18) are the major causative factors in cervical cancer (Bosch et al., 1995; Schiffman and Castle, 2003; zur Hausen, 1996). More than 90% of cervical cancer patients have been infected with these high-risk viruses that are capable of immortalizing and transforming normal human cells (Bosch et al., 1995). HPV16 and HPV18 are associated with high-grade squamous intraepithelial lesions; invasive cervical carcinomas (Slebos et al., 1995); and anal, peri-anal, vulvar, and penile cancers (zur Hausen, 2000). Two viral genes, *E6* and *E7*, are required for HPV16/18-mediated carcinogenesis (Munger et al., 1989).

The viral protein E6 induces p53 ubiquitination and degradation by complexing with E6 Associated Protein (E6AP), which is an E3 ligase (Scheffner et al., 1990, 1993). E6/E6AP-mediated degradation of p53 allows tumor cells to overcome cell cycle checkpoint control in DNA-damaged cells, contributing to the mutagenic and antiapoptotic effects of E6 (zur Hausen, 2000, 2002). E6 also facilitates degradation of the proapoptotic protein BCL2-antagonist/killer (BAK) (Thomas and Banks, 1998) and activates telomerase (Veldman et al., 2001).

HPV-induced malignant growth of cervical cancer depends upon continuous expression of E6. Although there are no specific therapies available, various approaches have been used in attempts to overcome E6-induced resistance to apoptosis. Antisense inhibition of the *E6* oncogene blocks the malignant phenotype of cervical cancer cells (von Knebel Doeberitz et al., 1992), and siRNAs targeting the viral *E6* oncogene mRNA effectively kill HPV-positive cancer cells (Butz et al., 2003). HPV16 E6 protein binding aptamers have been shown to eliminate HPV16-positive cancer cells by inducing apoptosis (Butz et al., 2000). While these approaches do lead to death of E6-expressing cells, they are unlikely to provide effective therapeutic agents in the near future.

SIGNIFICANCE

We have discovered compounds that increase doxorubicin's lethality in tumor cells that are relatively resistant to doxorubicin. These compounds can be used to reveal specific mechanisms for overcoming resistance of tumor cells to apoptosis-inducing drugs such as doxorubicin. To illuminate the mechanisms of action of these compounds, we designed both a pathway-based analysis and improved affinity probes for protein target identification. In addition, these doxorubicin-enhancing small molecules may be developed into adjuvant treatments for doxorubicin-resistant cancers.

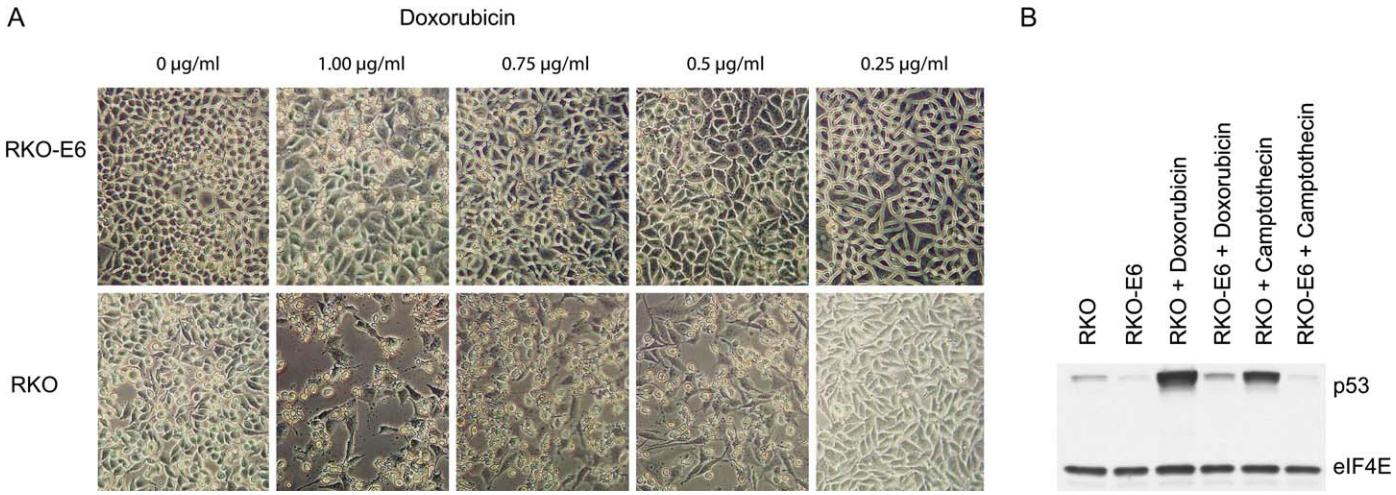

Figure 1. Differential effect of doxorubicin treatment on RKO and RKO-E6 cells

A: Cell viability assay: RKO and RKO-E6 cells were treated with doxorubicin for 16 hr to evaluate RKO-E6 cell resistance to doxorubicin. The largest differential in cell survival was observed at 0.50 μg/ml of doxorubicin. The high-throughput screen was performed in the presence of 0.50 μg/ml of doxorubicin. Compounds that restored doxorubicin-induced killing were further evaluated.

B: Western blot of p53: p53 cellular concentration is lower in the presence of E6 (see RKO and RKO-E6). Treatment with 0.5 μg/ml doxorubicin or camptothecin for 16 hr caused p53 to accumulate; in RKO-E6 cells, p53 accumulates to a lesser extent, due to E6/E6AP-mediated degradation. The blot was simultaneously probed with an antibody directed against eIF-4E to control for protein loading.

Small molecules, however, are more easily adaptable for therapeutic use than peptide or nucleic acid reagents, but few examples of small molecules that overcome E6-induced drug resistance have been described in the literature. The glycolytic pathway inhibitor 2-deoxyglucose (2-DG) has been reported to suppress transcription of HPV18 in cervical carcinoma cells (Maehama et al., 1998). The antioxidant pyrrolidine-dithiocarbamate (PDTC) suppresses HPV16 expression in human keratinocytes by modulating activity of the transcription factor AP-1 (Rosl et al., 1997). Dithiobisamine-based substances bind to the HPV16 E6 zinc finger and inhibit its activity (Beerheide et al., 2000). The histone deacetylase (HDAC) inhibitors sodium butyrate and trichostatin A induce G1/S phase arrest in HPV18-positive cervical carcinoma cells, followed by apoptosis, circumventing E6 antiapoptotic activity (Finzer et al., 2001, 2004). These examples suggest that it is possible to find small molecules that suppress HPV-induced tumorigenicity, although the reported examples lack specificity. Therefore, we sought to use small molecule screens (Smukste and Stockwell, 2005; Stockwell, 2000a, 2000b, 2004) to identify novel mechanisms and compounds for overcoming *E6*-induced resistance to apoptosis.

Results

In an attempt to identify compounds that overcome *E6*-induced drug resistance, we employed a cell-based model, the RKO colon carcinoma cell line (with high levels of p53), and an isogenic RKO-E6 cell line expressing the E6 oncoprotein. As expected, RKO-E6 cells have lower levels of p53 and fail to arrest in G1/S phase after various drug treatments (Slebos et al., 1995). We found that RKO-E6 cells are 2-fold to 4-fold more resistant to the anticancer drug doxorubicin compared to RKO cells (Figure 1). Doxorubicin is a DNA topoisomerase II-based DNA-damaging agent that induces double-strand DNA breaks, p53 stabilization, and apoptosis. Doxorubicin-treated RKO-E6 cells have lower levels of p53 than doxorubicin-treated RKO cells (Figure 1), suggesting that resistance to doxorubicin is caused, at least in part, by E6-induced degradation of p53. Thus, compounds that overcome E6-induced resistance should restore doxorubicin's lethality in RKO-E6 cells. We reasoned that such compounds might target E6, E6AP, p53, MDM2, or other proteins involved in the cellular response to doxorubicin.

In the primary screen, we identified compounds that inhibited proliferation of RKO-E6 cells in the presence of a dose of doxorubicin to which they were otherwise resistant. Cell viability was measured in 384-well format using Alamar Blue (Nociari et al., 1998), which is a fluorescent dye that detects cellular metabolic activity and correlates with cellular viability. RKO-E6 cells were treated with 4 μg/ml of each test compound, corresponding to 10 μM for a compound with a molecular weight of 400, and 0.5 μg/ml (0.9 μM) of doxorubicin for 24 hr. Each compound was tested in three replicates. We tested compounds in our *a*nnotated *c*ompound *l*ibrary (ACL; 2214 compounds) (Root et al., 2003); the NINDS library of 1040 compounds (Lunn et al., 2004); and our TIC library (Kelley et al., 2004), which encompasses 23,685 natural products, natural product analogs, and synthetic compounds (all tested compound structures and all activity data are provided in the Supplemental Data available with this article online). We identified 208 compounds from the TIC library that caused at least 25% reduction in Alamar Blue fluorescence in RKO-E6 cells in the presence of 0.5 μg/ml of doxorubicin, and 70 compounds from ACL and NINDS libraries that induced at least 30% RKO-E6 cell growth inhibition in the presence of 0.5 μg/ml of doxorubicin. We reasoned that among these 278 compounds there should be compounds that are not lethal on their own but restore sensitivity of RKO-E6 cells to doxorubicin.

To identify such compounds, we performed a secondary screen in which 272 of the primary hit compounds were tested in 2-fold dilution series in RKO cells in the absence of doxorubicin and in RKO-E6 cells in the presence of doxorubicin (the protocol for the screen, the tested compounds, and all activity data are provided in the Supplemental Data). This screen allowed us

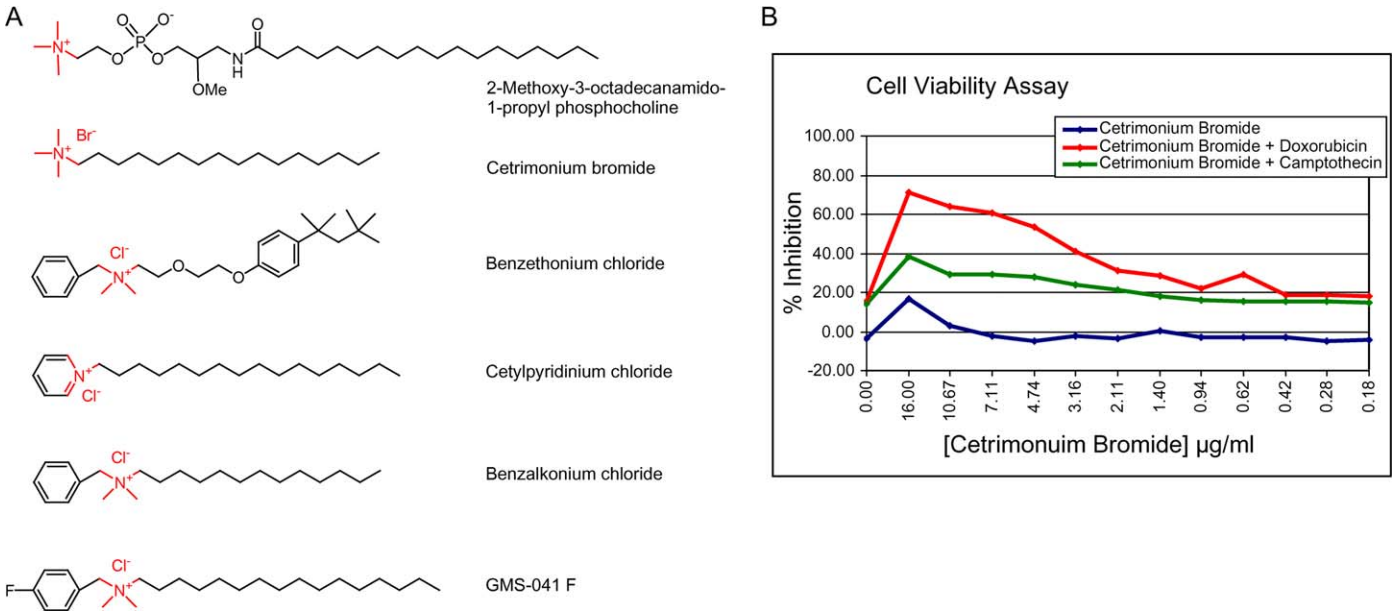

Figure 2. Quaternary ammonium compounds that enhance doxorubicin lethality

A: Structures of quaternary ammonium compounds (QACs) that selectively upregulated doxorubicin's lethality in RKO-E6 cells. GMS-041F is an analog of benzalkonium chloride that has been reported to inhibit proliferation of several human cancer cell lines (Gastaud et al., 1998).

B: RKO-E6 cells were treated with cetrimonium bromide in the presence of 0.5 µg/ml doxorubicin or camptothecin for 24 hr in 384-well plates. Percent inhibition of cell proliferation, measured with Alamar Blue, is shown in the graph. The 20% growth inhibition at 0 µg/ml cetrimonium bromide represents the toxicity of 0.5 µg/ml doxorubicin alone or 0.5 µg/ml camptothecin alone in RKO-E6 cells.

to eliminate compounds that are equally lethal to RKO cells in the absence of doxorubicin; such a filter should eliminate compounds that induce cell death via pathways independent of E6 and doxorubicin. We selected 88 compounds for further analysis that exhibited at least 20% greater cell growth inhibition in RKO-E6 cells in the presence of doxorubicin compared to the lethality of these compounds alone in RKO cells.

Compounds that overcome *E6*-induced doxorubicin resistance might act by upregulating p53. Thus, all 88 compounds were tested for their ability to upregulate p53 in RKO-E6 cells using Western blotting. Only one of the 88 compounds (designated T86N7) triggered a moderate ~50% upregulation of p53 (the structure and activity of this compound are provided in the Supplemental Data), indicating that most compounds restored doxorubicin lethality without directly inhibiting E6AP or E6 or even upregulating p53 by other means. This compound, T86N7, showed inconsistent activity in subsequent viability tests and showed no selective activity in a number of other cancer cell lines and therefore was not investigated further. Overall, we were surprised to find that overcoming the effect of E6 on p53 protein levels is difficult using a small molecule screening approach. However, given that all 88 of these compounds increased the sensitivity of RKO-E6 cells to doxorubicin (modestly or profoundly), we sought to uncover the basis for their desired resensitization activity.

To further group the 88 compounds based on their mechanism of action, we developed a pathway-based analysis using a cotreatment strategy. For these assays, we selected the microtubule inhibitor podophyllotoxin, the topoisomerase I-based DNA-damaging agent camptothecin, and doxorubicin itself. The antimitotic drug podophyllotoxin inhibits tubulin polymerization, leading to apoptosis, while camptothecin and doxorubicin recruit topoisomerase I and topoisomerase II, respectively, to introduce DNA strand breaks, which in return induce apoptosis. RKO-E6 cells were cotreated with selected compounds and with podophyllotoxin, camptothecin, or doxorubicin. Compounds that increased sensitivity to all three of these lethal compounds were assumed to act through general cell death mechanisms and were eliminated from further consideration. Compounds that enhanced sensitivity to both camptothecin and doxorubicin, but not podophyllotoxin, presumably operate downstream of the DNA damage response. Finally, compounds that synergized only with doxorubicin were likely to operate at the level of, or upstream of, topoisomerase II proteins.

For this tertiary screen, we selected the 24 most selective and active compounds from the secondary screen. Only a few representative compounds from each structural class of small molecules were tested. Each of these compounds was tested in four replicates in RKO and RKO-E6 cell lines alone, and with doxorubicin or podophyllotoxin (these compounds and activity data are provided in the Supplemental Data). Compounds that potentiated podophyllotoxin's toxicity were eliminated from further consideration, while compounds that confirmed their ability to selectivity increase doxorubicin's lethality in RKO-E6 and/or RKO cells were analyzed in more detail.

Below, we describe structurally and functionally related groups of compounds that emerged from these screens and candidate mechanisms of action.

Quaternary ammonium compounds

The first class of doxorubicin-enhancing agents comprised quaternary ammonium compounds (QACs), such as cetrimonium bromide, cetylpyridinium chloride, benzethonium chloride, and benzalkonium chloride. These compounds selectively increased doxorubicin's lethality in RKO-E6 cells but did not synergize with camptothecin (Figure 2). QACs have been reported to act as

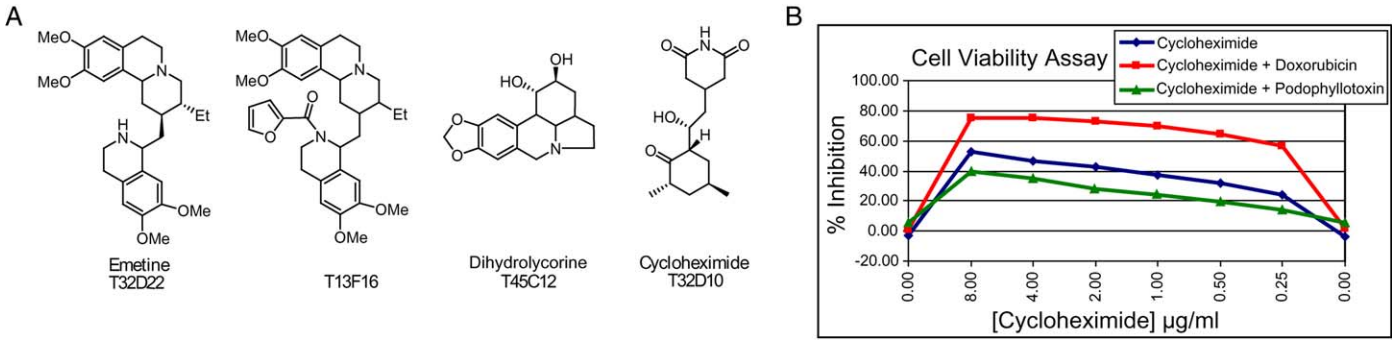

Figure 3. Protein synthesis inhibitors enhance doxorubicin lethality

A: Chemical structures of protein synthesis inhibitors that were found to enhance doxorubicin lethality.

B: Effect of cycloheximide on RKO-E6 cells in the presence of 0.5 μg/ml doxorubicin or 0.2 μg/ml podophyllotoxin. RKO-E6 cells were treated in 384-well plates for 24 hr. Percent inhibition of cell proliferation, measured with Alamar Blue, is shown in the graph.

membrane-disrupting agents by solubilizing the cytoplasmic membrane in bacteria and yeast. The ability of such compounds to disrupt the cytoplasmic membrane of tumor cells and increase their permeability could facilitate doxorubicin's uptake and lethality in RKO-E6 cells.

Benzalkonium salts have effects on a variety of cells (including T cells); downregulate tumor necrosis factor (TNF) expression; and are effective bactericidal, fungicidal, and virucidal agents with pleiotropic (direct and immunologically mediated) inhibitory activity against pathogens (Patarca and Fletcher, 1995; Patarca et al., 2000). Although these compounds have been primarily used as anti-infective agents, an analog of benzalkonium chloride has been reported to inhibit proliferation of several human cancer cell lines (Gastaud et al., 1998). These authors proposed that the ability of quaternary ammonium functional groups to act as alkylating agents might be responsible for their inhibitory effect on tumor cells. However, benzethonium chloride and benzalkonium chloride did not induce apoptosis in RKO-E6 cells in the absence of doxorubicin, casting doubt on this explanation. In addition, these compounds did not induce cell cycle arrest, which is typically caused by DNA alkylating agents, and did not upregulate p53, p21, or caspase 3, implying a different mechanism of activity (data not shown). These compounds may be fairly benign agents that could be used for overcoming resistance to doxorubicin.

Protein synthesis inhibitors

Cycloheximide, emetine, and dihydrolycorine potentiated doxorubicin's lethality in RKO-E6 cells, although at higher concentrations they exhibited lethality on their own (Figure 3). Protein synthesis inhibitors have been reported to sensitize cells to members of the TNF family (Choi et al., 2004) and to cisplatin (Budihardjo et al., 2000). Contrary to our observations, however, there are several reports that cycloheximide antagonizes doxorubicin-induced apoptosis (Bonner and Lawrence, 1989; Furusawa et al., 1995). It is likely that protein synthesis inhibition has diverse effects, depending on the concentrations used for treatment and the genetic makeup of the target cells.

Consistent with its reported inhibitory effects on protein synthesis, cycloheximide caused a disappearance of p53 and p21 in RKO-E6 cells, even when cotreated with doxorubicin. On the other hand, cycloheximide caused increased topoisomerase IIα levels in RKO-E6 cells. Protein synthesis inhibitors appear, somewhat unexpectedly, to constitute an effective class of agents for restoring doxorubicin lethality.

T13F16 is a close analog of emetine with modest activity in our viability studies (Figure 3 and data not shown). However, it appears to lack potent protein synthesis inhibitor activity and did not prevent upregulation of p53 and p21 in response to doxorubicin's treatment. This analog may have fewer undesired side effects than the more potent protein synthesis inhibitors.

11-deoxyprostaglandin E1

11-deoxyprostaglandin E1 analogs (e.g., T19I13) were isolated in the screen. Depending upon the amide functionality, these compounds exhibited a broad range of activity and selectivity, while the parent compound 11-deoxyprostaglandin E1 showed no activity in this screen (Figure 4 and data not shown). T19I13 induced late S/G2 phase arrest in RKO-E6 cells, while no changes in cell cycle were observed in RKO cells. Upon cotreatment with doxorubicin and T19I13, RKO-E6 cells accumulated in S/G2 phase, while RKO cells populated G1 and late S/G2 phase. T19I13 selectively increased doxorubicin's lethality, while not synergizing with podophyllotoxin or camptothecin. However, a rapid loss of activity of T19I13 (likely due to loss of the allylic hydroxyl functionality) in cell culture was observed, impeding further testing of this analog series. Thus, although these prostaglandin analogs have potent activity, their chemical instability renders them unsuitable for use as probes or drug candidates, unless more stable analogs can be generated.

1,3-bis(4-morpholinylmethyl)-2-imidazolidinethione and related analogs

1,3-bis(4-morpholinylmethyl)-2-imidazolidinethione (T55D7) and its analogs represent an unexplored class of small molecules. We found that, at low micromolar concentrations, these compounds increased both doxorubicin's and camptothecin's lethality in RKO and RKO-E6 cells (Figure 5A). T55D7 was studied in more detail as a prototypical member of this compound class; it upregulated doxorubicin's potency in other cell lines: HeLa, TC32, and A673. However, T55D7 did not increase the microtubule inhibitor podophyllotoxin's lethality, indicating a DNA damage-related mechanism of action. Only at very high concentrations (30–100 μM) did T55D7 and its analogs exhibit doxorubicin-independent lethality (Figure 5A). To investigate whether T55D7 truly synergizes with doxorubicin, we treated RKO,

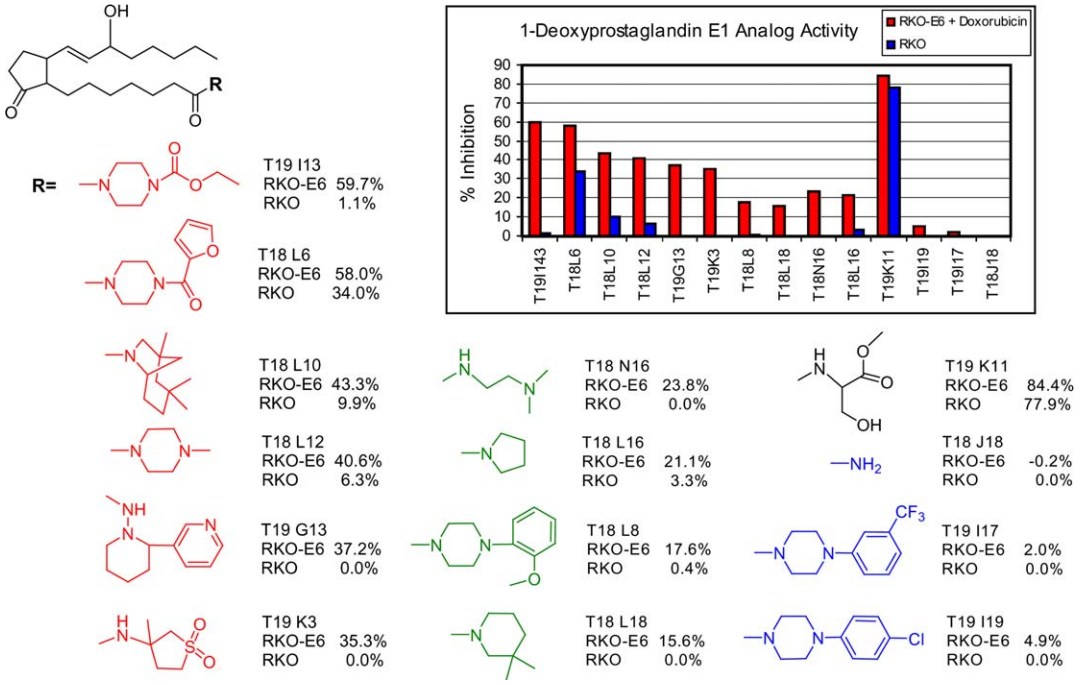

Figure 4. 11-deoxyprostaglandin E1 analogs that enhance doxorubicin lethality

RKO cells were treated with 8 μg/ml of each 11-deoxyprostaglandin E1 analog, and RKO-E6 cells were treated with 8 μg/ml of 11-deoxyprostaglandin E1 analog and 0.5 μg/ml of doxorubicin. The percent inhibition of cell proliferation is shown and listed next to each analog. Amide functionalities are colored based on their activity: active and selective analogs, red; moderately active and selective analogs, green; toxic analogs, black; and inactive analogs, blue.

RKO-E6, HeLa, and TC32 cell lines with a combination dose matrix of T55D7 and doxorubicin (Figure 5C). The Bliss independence model predicts the combined response C for two single compounds with effects A and B according to the relationship C = A + B − A*B and represents one of the most stringent requirements for synergy (Keith et al., 2005). According to this model, the excess over predicted Bliss independence represents the synergistic effect of the combination treatment at a given pair of concentrations. Based on this analysis, T55D7 exceeded Bliss independence with doxorubicin at multiple doses; the most significant potentiation of doxorubicin's lethality was found in RKO-E6 cells (Figure 5C and Supplemental Data).

Surprisingly, Western blot analysis of RKO-E6 cells cotreated with doxorubicin and T55D7 analogs showed no changes in p53, p21, or MDM2 levels, compared to doxorubicin-treated cells. T55D7 and its analogs also did not change p53 concentration in the absence of doxorubicin, implying that the ability of these compounds to potentiate doxorubicin's toxicity is not caused by their ability to induce DNA damage or affect processes upstream of 53.

Notably, T55D7 treatment resulted in pronounced S phase arrest in RKO-E6 cells, while virtually no changes in the cell cycle were observed in RKO cells (Figure 5B). When RKO and RKO-E6 cells were cotreated with T55D7 and doxorubicin, we observed a broadening of the G2 phase and an increase in S phase in RKO-E6 cells, while RKO cell cycle distribution was similar to doxorubicin-only treatment. Thus, T55D7 and related analogs have the ability to enhance the lethality of DNA-damaging agents in numerous tumor cell lines. These compounds might be developed into adjuvant therapies for doxorubicin and other DNA-damaging agents.

Indoxins

T13M9 and T20D5 are representatives of a group of compounds that we named indoxins for their ability to *in*crease *dox*orubicin's lethality selectively. These small molecules selectively increased doxorubicin's lethality in RKO, RKO-E6, HeLa, and TC32 cells, while showing no synergy with camptothecin or podophyllotoxin. A Bliss independence analysis showed that indoxins and doxorubicin have synergistic effects in all four cell lines (Figure 6E and Supplemental Data). This doxorubicin selectivity implied a topoisomerase II-related mechanism of action. Indeed, direct upregulation of topoisomerase IIα was detected in RKO and RKO-E6 cells treated with indoxin A and indoxin B using Western blotting (Figure 6C). Interestingly, indoxins also induced S phase arrest in RKO-E6 cells, while not affecting the cell cycle distribution of RKO or HeLa cells (Figure 6D). Topoisomerase IIα is upregulated during S phase and G2/M phases. However, since increased topoisomerase IIα levels were observed in RKO and RKO-E6 cells, but S phase arrest was only seen in RKO-E6 cells, these two events seems to be independent in this assay system.

A series of indoxin analogs were synthesized to assess functionalities necessary for their activity. Structure-activity analysis of indoxin analogs revealed that an acyl group must be present on the secondary amine for activity to be observed. However, when the acetyl or propanoyl functionality was substituted with a biotin-linked acyl group, indoxin A retained some activity and selectivity, indicating that larger substituents can be introduced at this site (Figure 6 and Supplemental Data).

To analyze further indoxins' mechanisms of action, we embarked on the development of indoxin affinity probes for protein target identification. Initially, we synthesized a series of biotin-

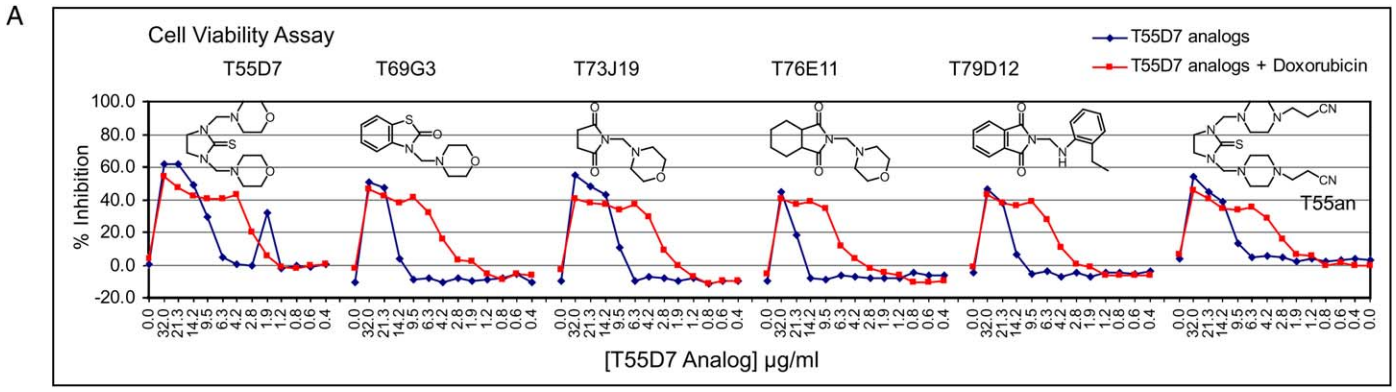

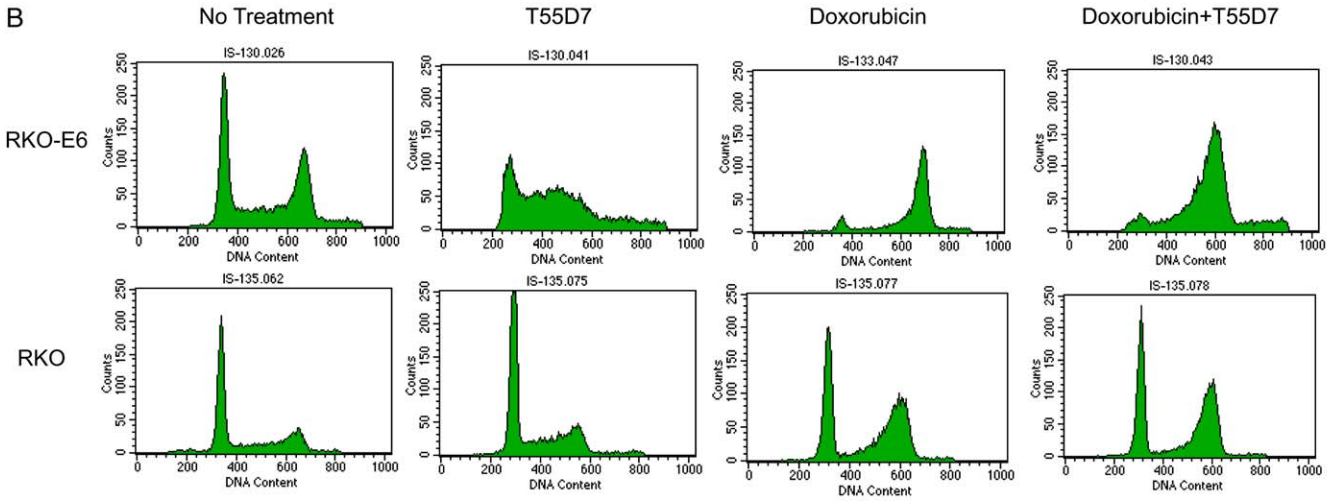

C

Percent Inhibition: T55D7, RKOE6 cells

[Doxorubicin] µg/ml	1.19	0.79	0.53	0.35	0.24	0.16	0.10	0.00	[T55D7] µg/ml
	67	70	70	69	53	21	3	0	9.00
	69	73	71	42	18	7	2	0	6.00
	67	64	56	22	9	4	1	0	4.00
	71	59	42	10	6	0	1	1	2.67
	71	56	29	8	7	0	0	0	1.78
	68	50	23	3	2	-5	-3	-2	1.19
	67	49	17	5	4	-3	-2	-1	0.79
	65	45	16	6	6	-1	-2	0	0.53
	66	46	15	9	6	2	-2	0	0.35
	66	43	18	10	7	2	0	0	0.23
	59	43	21	11	10	6	1	1	0.16
	57	37	16	9	9	2	1	0	0.00

Excess over Bliss Independence: T55D7, RKOE6 cells

[Doxorubicin] µg/ml	1.19	0.79	0.53	0.35	0.23	0.16	0.00	[T55D7] µg/ml
	9	33	54	59	44	18	0	9.00
	11	37	55	33	9	5	0	6.00
	9	27	40	12	0	1	0	4.00
	13	22	26	0	-4	-3	0	2.67
	13	19	13	-1	-2	-2	0	1.78
	11	15	9	-5	-5	-5	0	1.19
	10	13	3	-3	-4	-4	0	0.79
	8	9	0	-3	-3	-3	0	0.53
	8	9	0	0	-3	0	0	0.35
	8	7	2	1	-2	0	0	0.23
	2	6	5	2	0	4	0	0.16
	0	0	0	0	0	0	0	0.00

Figure 5. T55D7 and related analogs enhance doxorubicin lethality

A: RKO-E6 cells were treated with T55D7 and its analogs in the presence or absence of 0.5 µg/ml doxorubicin for 24 hr. Percent inhibition of cell proliferation, measured with Alamar Blue, is shown in the graph.

B: T55D7 induces S phase arrest in RKO-E6 cells, but not in RKO cells. RKO and RKO-E6 cells were treated with 4 µg/ml T55D7 alone or with 0.5 µg/ml doxorubicin for 24 hr and stained with propidium iodide; the cell cycle distribution was determined using flow cytometry.

C: A combination dose matrix, showing the combined effect of T55D7 and doxorubicin, in RKO-E6 cells. The experimentally measured cell growth inhibition (with the Alamar Blue assay) is shown for each concentration. The calculated excess inhibition over the predicted Bliss independence model indicates the synergy between indoxin B and doxorubicin treatment. The predicted Bliss independence effect was subtracted from the experimentally measured cell growth inhibition at each pair of concentrations. The color of the squares indicates the level of activity in excess of that predicted by Bliss independence.

derivatized indoxin affinity probes I–III (Figures 7 and 8). Biotin provides a small, high-affinity tag for resin-based target protein pull-down (Hermanson, 1996). We prepared RKO-E6 cell lysates in a nondenaturing lysis buffer, incubated them with the indoxin-biotin probes for 12–16 hr at 4ºC, and then passed these cell lysates over NeutrAvidin beads. The bound proteins were eluted by boiling NeutrAvidin beads in SDS page buffer; resolving on Tris-glycine acrylamide gels; and staining with Coomassie blue, silver, or SYPRO Ruby (Molecular Probes) stains. However, no selective protein targets were isolated using these probes. We reasoned that, since indoxins are active at micromolar concentrations and have no functional groups that could form a covalent bond with their protein targets, they provide insufficient affinity for direct target identification.

However, we reasoned that incorporation of a photo-activatable functionality that allows for covalent bond formation between a small molecule affinity probe and its target protein may enhance the likelihood of protein target identification (Dorman and Prestwich, 2000; Weber and Beck-Sickinger, 1997). Benzophenone photoprobes have become the group of choice for high-efficiency photo-covalent modifications of binding proteins in vitro (Dorman and Prestwich, 1994; Prestwich et al., 1997), and we suspected they might be useful in cells as well. We used *p*-benzoyl-L-phenylalanine (L-Bpa) to incorporate a benzophenone moiety in the biotin-tagged photoreactive indoxin probe IV (Figure 8). We also prepared the biotin-tagged photoreactive probe V lacking indoxin functionality as a negative control (Figure 8). The RKO-E6 cell lysates were incubated with the photoreactive probes and irradiated with 350 nm ultraviolet light. Proteins crosslinked to these probes were purified using NeutrAvidin beads and eluted with SDS buffer. A number of nonspecific bands were observed in both the indoxin probe and control probe pull-downs (Figure 7D) that may be due to crosslinking to biotin binding proteins.

We reasoned that biotin-induced crosslinking to the indoxin photoprobe could be substantially reduced if the biotin affinity tag were replaced with a nonnatural affinity tag that does not have high-affinity cellular targets. A number of antibodies have been developed against fluorescein, providing a convenient route for the resin-based isolation of protein targets using fluorescein as an affinity tag. We thus prepared indoxin-benzophenone-fluorescein photoreactive probe VI (Figure 8). Protein targets crosslinked to these probes were purified by immobilizing fluorescein on protein A-containing resin with an anti-fluorescein antibody. The proteins were specifically eluted with excess fluorescein or with low-pH buffer. The fluorescein affinity tag indeed reduced nonspecific crosslinking to the control probe VII (Figure 7D). We used this fluoresceinated indoxin probe for a large-scale protein pull-down using both nuclear and cytoplasmic fractions of RKO-E6 cell lysates. Purified proteins were sequenced using liquid chromatography/tandem mass spectrometry (LC-MS/MS). Using the indoxin-fluorescein photolabel, we identified a number of proteins that had at least three corresponding peptide sequences in the MS data. In order to determine which of these proteins are specific for binding indoxin, we performed identical experiments for the control probe VII, lacking indoxin. We found five proteins that were selectively pulled down with the indoxin probe (Figure 7E) from the nuclear fraction.

To confirm these findings, we repeated the pull-down with the indoxin probe and identified two proteins that were again selectively pulled down with indoxin A from the nuclear fraction. The actin-related proteins myosin 1C and ARP2 were both repeatedly pulled down with indoxin probes from the nuclear fraction but were not present in the control pull-down experiments. Thus, a nuclear actin-related protein complex involving myosin 1c and ARP2 is a candidate target for mediating the effects of indoxins.

Discussion

In our cell-based viability screen, we identified several groups of compounds that potentiate doxorubicin's lethality in E6-expressing tumor cells, thus overcoming E6-induced drug resistance. We discovered that the major mechanisms for increasing doxorubicin's lethality in E6-expressing tumor cells are (1) upregulation of topoisomerase IIα and (2) induction of S phase arrest. Topoisomerase IIα is regulated in proliferation-dependent and cell cycle-dependent manner (Chow and Ross, 1987; Larsen and Skladanowski, 1998). The level of topoisomerase IIα increases during S phase and reaches the highest concentration during late G_2/early M phase. In addition, topoisomerase-IIα-mediated drug sensitivity markedly increases during S phase (Chow and Ross, 1987). Thus, compounds that induce S phase arrest should potentiate doxorubicin's lethality. Moreover, there is ample evidence that topoisomerase-targeting drug potency is directly related to the expression levels of the topoisomerases (Asano et al., 2005; Houlbrook et al., 1996; Kellner et al., 2002; Koshiyama et al., 2001; MacGrogan et al., 2003). Thus, compounds that directly upregulate topoisomerase levels in tumor cells should potentiate topoisomerase-targeting drugs.

In this study, we identified a group of compounds (indoxins) that both upregulate topoisomerase IIα and induce S phase arrest in RKO-E6 cells. Indoxin probes repeatedly and selectively pulled down myosin 1C from the nuclear fraction of the RKO-E6 cells. The nuclear isoform of myosin 1C (NMI) shares more than 98% sequence homology with cytoplasmic myosin 1C (Pestic-Dragovich et al., 2000). Although LC-MS/MS analysis of the isolated sequences is not sufficient for distinguishing between the nuclear and cytoplasmic myosin 1C, the protein was isolated from the nuclear fraction of RKO-E6 cells and presumably is the nuclear isoform.

Given that indoxins upregulate topoisomerase IIα in both RKO and RKO-E6 cells but only cause S phase arrest in RKO-E6 cells, these two mechanisms can be dissociated. We believe, therefore, that indoxins are dual-action compounds that cause these two distinct effects (topoisomerase IIα upregulation and S phase arrest) and that they both contribute to increased doxorubicin sensitivity. The Bliss independence analysis supports this dual-mechanism hypothesis by demonstrating that indoxins showed greater combination effect with doxorubicin in RKO-E6 cells than in RKO or HeLa cells. The ability of indoxins to inhibit nuclear myosin 1C could mediate topoisomerase IIα transcriptional upregulation, as nuclear myosin 1C has been linked to transcriptional control (see below). A cytosolic myosin target might mediate the S phase-arresting activity of indoxins. Both activities should contribute to the increased sensitivity of indoxin-treated cells to doxorubicin.

Nuclear myosin 1C colocalizes with RNA polymerase II and may affect transcription (Pestic-Dragovich et al., 2000). Nuclear actin and myosin 1C (NMI) are associated with rDNA and are required for RNA polymerase I transcription (Pestic-Dragovich et al., 2000). Depletion or inhibition of nuclear myosin 1C or actin results in decreased nucleolar transcription, while overexpression of NMI amplifies pre-rRNA synthesis (Pestic-Dragovich et al., 2000). Thus, there is ample precedent for our hypothesis that nuclear myosin 1c could regulate topoisomerase IIα expression.

In summary, we have found that the most tractable mechanism for overcoming doxorubicin resistance is upregulation of the direct target of doxorubicin, topoisomerase IIα. In addition, induction of S phase arrest potentiates the cytotoxicity of topoisomerase IIα-mediated DNA damage. Each of these mechanisms provides modest potentiation of doxorubicin's lethality. For example, cotreatment of RKO-E6 cells with hydroxyurea (a compound that arrests cells in S phase) and doxorubicin

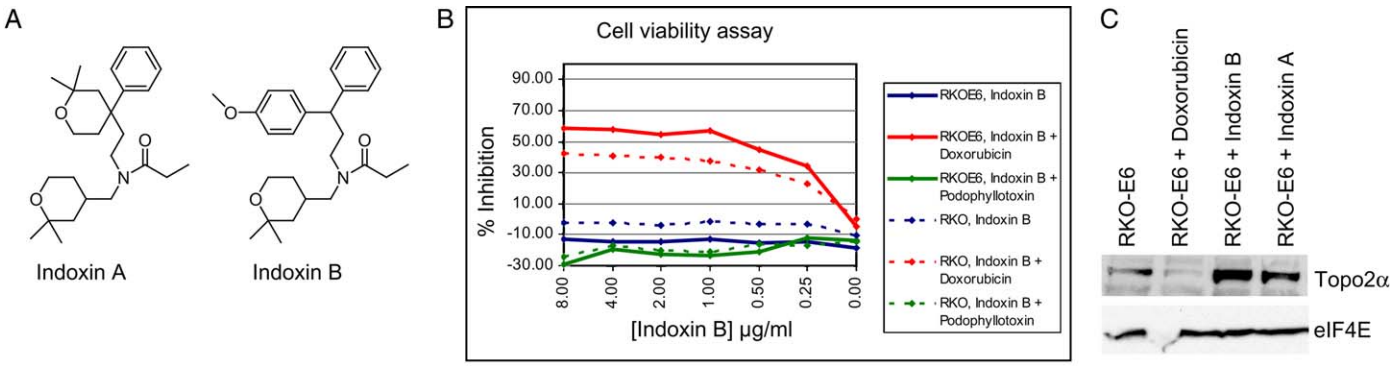

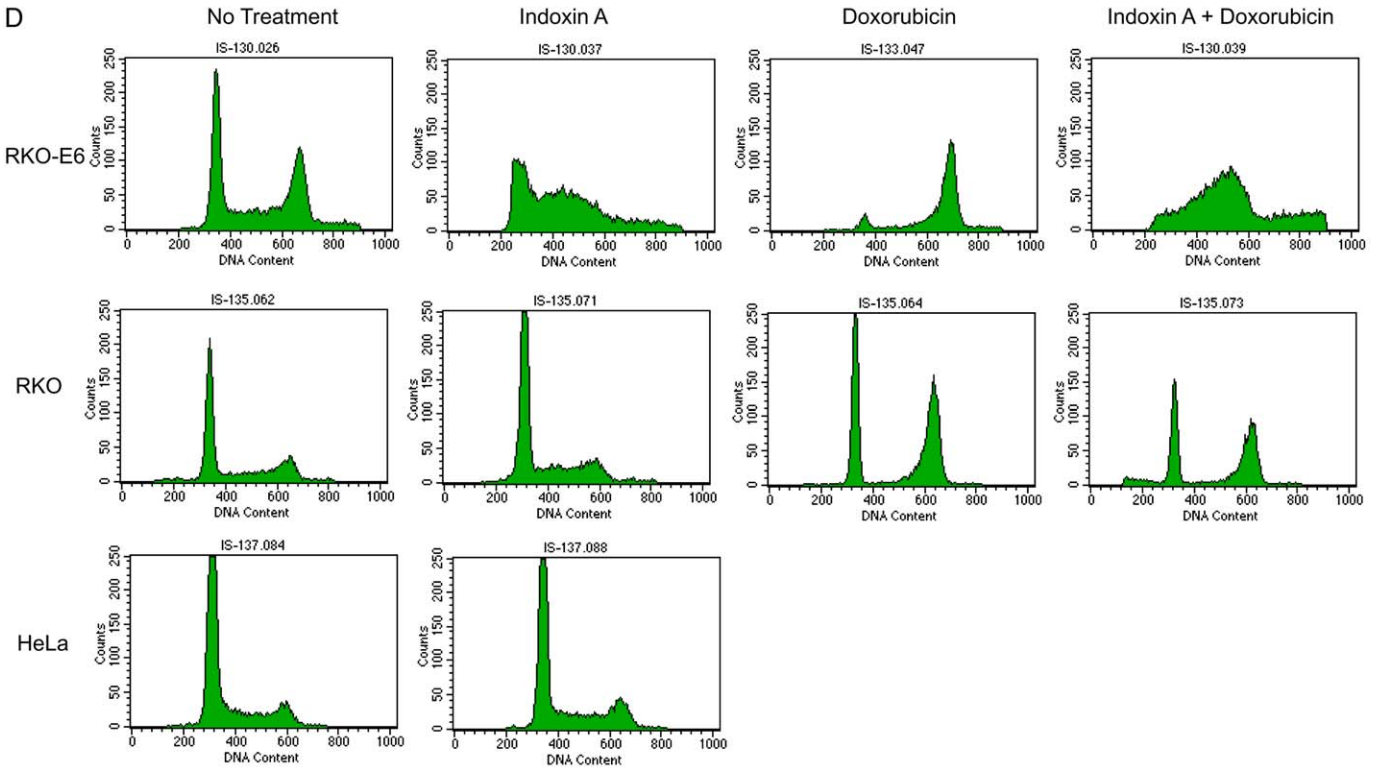

E

Percent Inhibition: Indoxin B, RKOE6 cells

[Doxorubicin] µg/ml	1.19	0.79	0.53	0.35	0.24	0.16	0.10	0.00	[Indoxin] µg/ml
	84	83	65	38	5	3	2	0	9.00
	82	84	70	39	6	5	3	2	6.00
	76	78	66	22	4	2	0	0	4.00
	77	69	61	18	3	-1	0	-1	2.67
	73	69	50	11	3	-2	-2	-2	1.78
	69	65	49	6	1	-5	-5	-2	1.19
	68	61	38	4	3	-5	-4	-3	0.79
	67	50	26	3	3	-3	-4	-4	0.53
	68	48	14	5	3	-1	-4	-3	0.35
	66	42	12	7	4	-2	-4	-3	0.23
	61	41	17	9	6	2	-2	-2	0.16
	57	32	13	9	6	-2	-3	-2	0.00

Excess over Bliss Independence: Indoxin B, RKOE6 cells

[Doxorubicin] µg/ml	1.19	0.79	0.53	0.35	0.23	0.16	0.00	[Indoxin] µg/ml
	28	51	52	30	0	5	0	9.00
	25	51	55	29	-2	5	0	6.00
	19	45	53	13	-2	4	0	4.00
	20	37	49	10	-2	2	0	2.67
	18	39	39	5	-1	2	0	1.78
	13	34	38	-1	-2	-1	0	1.19
	13	31	27	-2	0	0	0	0.79
	12	21	16	-2	0	2	0	0.53
	13	18	3	-1	0	4	0	0.35
	11	12	2	1	1	3	0	0.23
	5	9	4	1	0	4	0	0.16
	0	0	0	0	0	0	0	0.00

Figure 6. Indoxins enhance doxorubicin lethality

A: Chemical structures of indoxin A and indoxin B.

B: Indoxin-B-treated RKO and RKO-E6 cells in the presence of 0.5 μg/ml doxorubicin or 0.2 μg/ml podophyllotoxin. RKO and RKO-E6 cells were treated in 384-well plates for 24 hr. Percent inhibition of cell proliferation, measured with Alamar Blue, is shown in the graph.

C: RKO-E6 cells were treated with 0.5 μg/ml doxorubicin, 4 μg/ml indoxin A, or 4 μg/ml indoxin B for 24 hr, and the level of topoisomerase IIα was determined by Western blot. The membrane was reprobed for eIF4E as a loading control.

D: RKO, RKO-E6, or HeLa cells were treated with 4 μg/ml of indoxin A alone and/or with 0.5 μg/ml doxorubicin for 24 hr. Cells were stained with propidium iodide, and the cell cycle distribution was determined using flow cytometry.

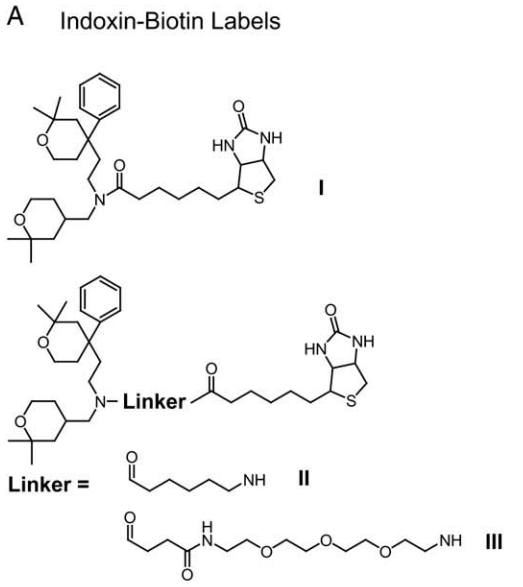

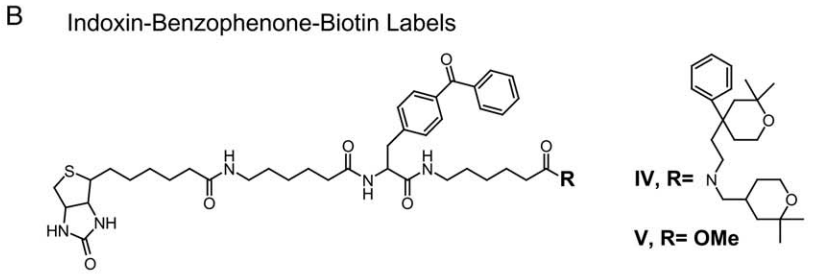

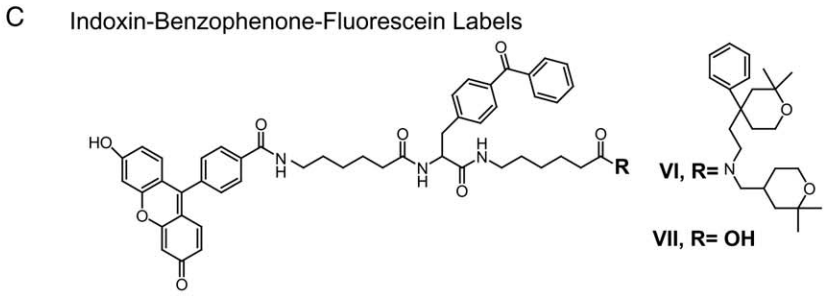

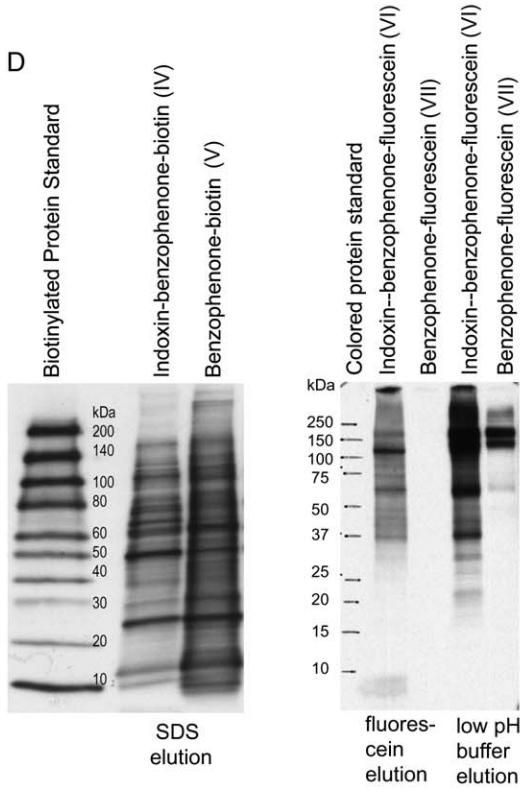

E Proteins selectively isolated with Indoxin-Benzophenone-Fluorescein probe:

Protein	MW	Localization
DDB1, DNA damage binding protein 1	126968	Nuclear
MYO1C, myosin IC	118038	Nuclear and cytoplasmic
ACTN4, alpha-actinin 4	104854	Nuclear and cytoplasmic
SND1, staphylococcal nuclease domain containing protein 1	101997	Nuclear and cytoplasmic
ARP2, actin-like protein 2	44761	Cytoplasmic

Figure 7. Indoxin affinity probes

A: Structures of indoxin-biotin labels.

B: Structures of indoxin-benzophenone-biotin labels.

C: Structures of indoxin-benzophenone-fluorescein labels.

D: Proteins isolated using indoxin and control probes; nonspecific crosslinking was observed using the benzophenone-biotin control probe. Replacement of biotin with fluorescein as an affinity tag reduced nonspecific crosslinking.

E: Proteins that were selectively isolated using the indoxin-benzophenone-fluorescein probe, but not the control benzophenone-fluorescein probe. Myosin 1C and ARP2 were repeatedly identified in this manner.

E: A combination dose matrix, showing the combined effect of indoxin B and doxorubicin in RKO-E6 cells. The experimentally measured cell growth inhibition (Alamar Blue assay) is shown for each concentration. The calculated excess inhibition over the predicted Bliss independence model indicates the synergy between indoxin B and doxorubicin treatment. The predicted Bliss independence effect was subtracted from the experimentally measured cell growth inhibition at each pair of concentrations. The color of the squares indicates the level of the synergy.

Synthesis of Indoxin-Biotin Probes

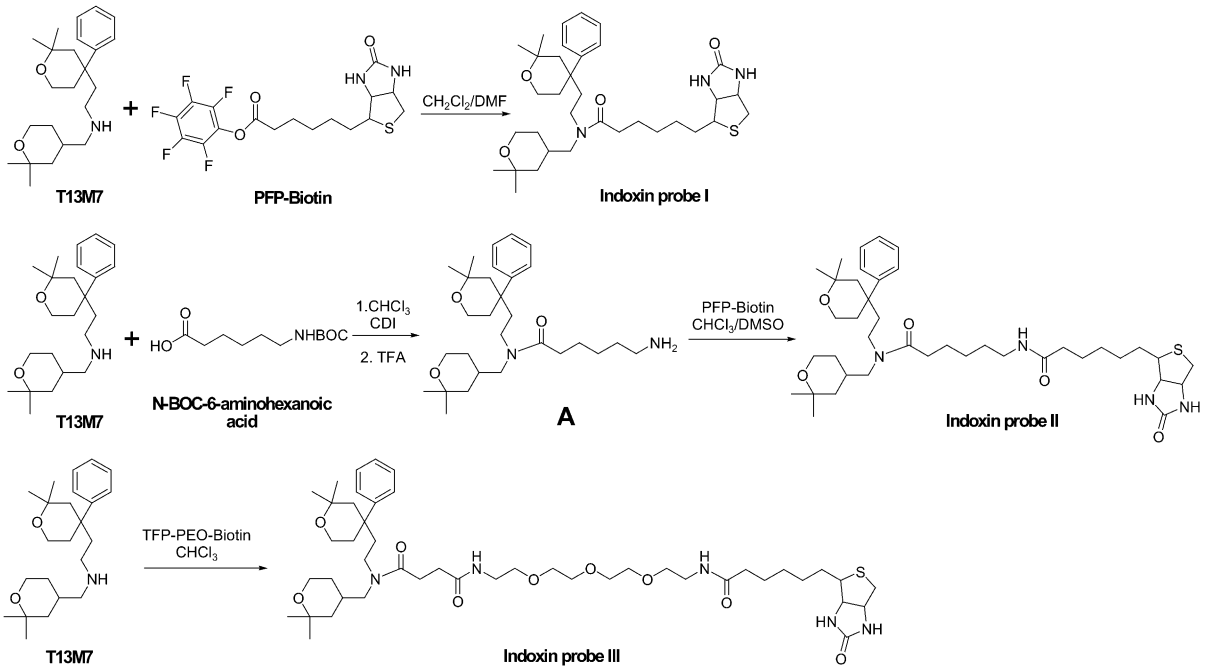

Synthesis of Indoxin-Benzophenone-Biotin Probes

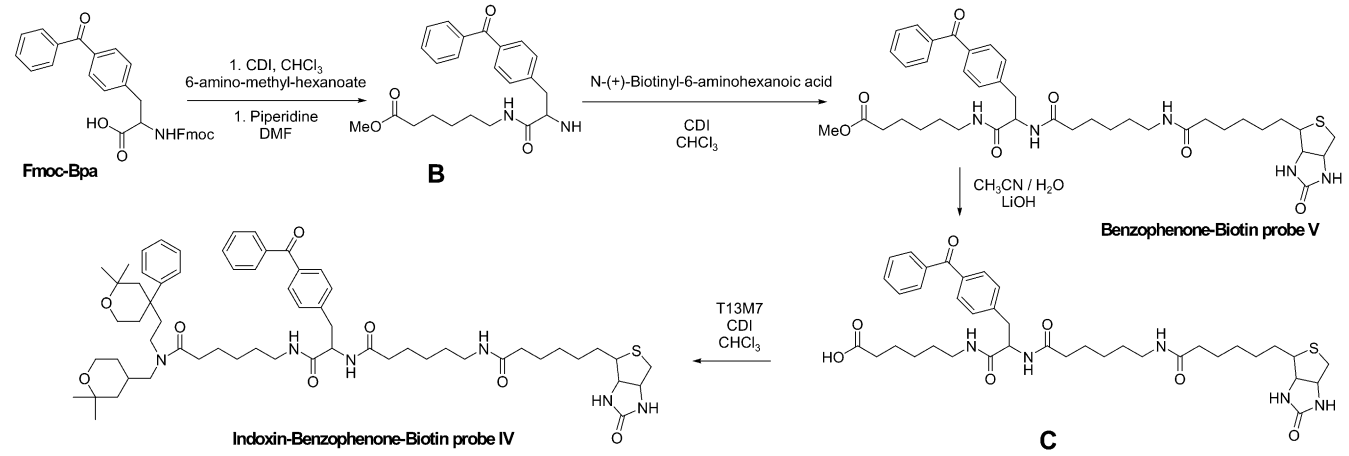

Synthesis of Indoxin-Benzophenone-Fluorescein Probes

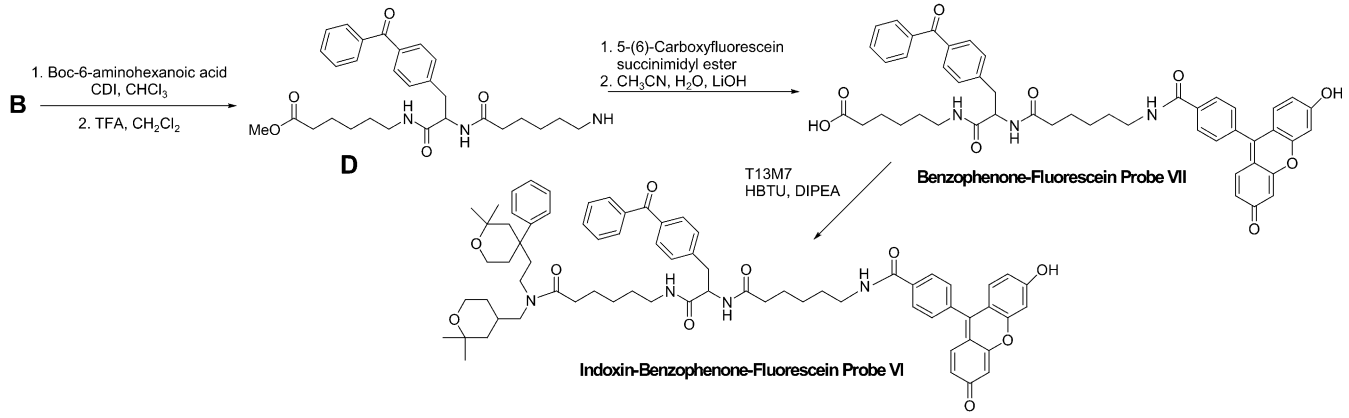

resulted in only modest upregulation of doxorubicin's lethality (data not shown). However, compounds that drive both of these mechanisms result in a strong sensitization effect.

Experimental procedures

Cell lines

RKO colon carcinoma cells (ATCC, order #CRL-2577) and RKO-E6 colon carcinoma cells transfected with HPV E6 inserted in pCMV.3 (ATCC, order #CRL-2578) were grown in MEM with 2 mM L-glutamine and Earle's BBS adjusted to contain 1.5 g/l $NaHCO_3$, 0.1 mM nonessential amino acids, and 1.0 mM sodium pyruvate and supplemented with 10% fetal bovine serum, penicillin, and streptomycin (pen/strep). Both cell lines were incubated at 37ºC in a humidified incubator containing 5% CO_2.

Compound libraries

Our ACL comprising 2214 compounds, the NINDS library of 1040 compounds obtained from the National Institute of Neurological Disorders and Stroke, and our TIC library comprised of 12,960 synthetic compounds (Chembridge) and 10,725 natural products and their analogs (IBS and TimTec) were used in the primary screen. All compound libraries were prepared as 4 mg/ml solutions in DMSO in 384-well polypropylene plates and stored at −20ºC.

Benzalkonium chloride (cat. #234427, MW), benzethonium chloride (cat. #B-8879, MW 448.1), D-biotin (cat. #B-4501, MW 244.3), S-(+)-camptothecin (cat. #C9911, 348.4), cetyltrimethylammonium bromide (cat. #855820, MW 364.46), cycloheximide (C-76798, MW 281.4), doxorubicin (cat. #D-1515, MW 580.0), hexadecylpyridinium chloride monohydrate (cat. #C9002, MW 358.01), hydroxyurea (cat. #H-8627, MW 76.05), and podophyllotoxin (cat. #P-4405, MW 414.4) were obtained from Sigma-Aldrich. Indoxin A (MW 415.61) and indoxin B (MW 423.59) were obtained from Interbioscreen Ltd.

Compound designation

Each hit compound from the primary screen was assigned a designation based on the location of this compound in the libraries. For example, the designation T86N7 indicates that compound is located on the *T*IC library's mother plate number *86*, row *N*, column *7*.

Screening

Daughter replica plates were prepared with a Zymark Sciclone ALH by diluting DMSO stock plates 50-fold in medium lacking serum and penicillin/streptomycin to obtain a compound concentration in daughter plates of 80 μg/ml with 2% DMSO. Assay plates were prepared by seeding cells in black, clear-bottom 384-well pates (Corning Inc., cat. #3712). Columns 3–22 were treated with compounds from a daughter library plate by transferring 3 μl from the daughter library plate using 384-position fixed cannula array. The final compound concentrations in assay plates were 4 μg/ml.

Primary screen: Alamar Blue viability assay

The Alamar Blue assay incorporates a fluorimetric/colorimetric growth indicator that changes color in the response to chemical reduction by viable cells (Nociari et al., 1998). Cells were seeded at a density of 3000 cells (57 μl) per well in 384-well black, clear-bottom plates using a syringe bulk dispenser (Zymark Sciclone ALH). Three microliters were removed from a compound daughter plate using a 384 fixed cannula head and added to the assay plate, making the final concentration of each compound 4 μg/ml. The plates were incubated for 24 hr at 37ºC. Ten microliters of 40% Alamar Blue (Biosource Int., cat. #DAL1100) solution in media was added to each well (1:10 dilution). The assay plates were incubated for 16 hr. Fluorescence intensity was determined using a Packard Fusion platereader with a 535 nm excitation filter and a 590 nm emission filter. The average fluorescence for the whole plate was used as a positive control. Average percentage inhibition for each well was determined using our freely available SLIMS software (Kelley et al., 2004).

Retesting of compounds in a dilution series

The daughter plates for the 2-fold dilution series were prepared with a Zymark Sciclone ALH by diluting the replica daughter plates to obtain compound concentrations from 8 μg/ml–0.008 μg/ml (columns 8–18). Columns 1–7 were used as untreated control. RKO-E6 cells were seeded at the density of 3000 per well in 55 μl, and 5 μl was added from the daughter plate. RKO cells were seeded at the density of 2000 per well in 55 μl, and 5 μl were added from the daughter plate. The assay was incubated for 24 hr at 37ºC. Ten percent Alamar Blue was added to each well, and the assay was incubated for 16 hr (see above).

Compounds for retesting were purchased from the manufacturers or from Sigma-Aldrich (see above). Stocks were prepared in DMSO at 4 mg/ml.

Bliss independence analysis

Each cell line (RKO, RKO-E6, HeLa, and TC32) was treated with a dose combination matrix of doxorubicin and a selected hit compound. Each treatment was done in a triplicate in 384-well format. The average percent inhibition of cell proliferation, measured with Alamar Blue, was determined using the following formula:

$$\text{Percent inhibition} = (1 - (X - N)/(P - N))$$

X, the average fluorescence readout for each treatment; N, the negative control signal (in the absence of any cells); P, the positive control (the average fluorescence readout of untreated cells).

The predicted Bliss additive effect was determined using the following formula:

$$C = A + B - A*B$$

C, the combined response for two single compounds with effects A and B; A, the percent inhibition of compound A at the particular concentration; B, the percent inhibition of compound B at the particular concentration.

The excess over predicted Bliss independence was calculated by subtracting the predicted Bliss effect for each treatment from the experimentally determined percent inhibition for the same treatment.

Western blot analysis

Antibodies were obtained from the indicated suppliers: p53 (Oncogene/Calbiochem, cat. #OP43), p21 (Santa Cruz Biotechnology Inc., cat. #sc-817), MDM2 (Santa Cruz Biotechnology Inc., cat. #sc-965), topoisomerase IIα (TopoGEN, cat. #2011-1), topoisomerase I (BD PharMingen, cat. #556597), Cyclin B (BD Transduction Laboratories, cat. #610219), Cyclin A (BD Transduction Laboratories, cat. #611268), anti-fluorescein-HRP (Molecular Probes, cat. #A21253), anti-biotin-HRP (Cell Signaling Technology, cat. #7075; Jackson ImmunoResearch Laboratories, cat. #200-032-096), eIF4E (Santa Cruz Biotechnology Inc., cat. #sc-9976 HRP).

Cells were lysed in denaturing lysis buffer (50 mM HEPES KOH [pH 7.4], 40 mM NaCl, 2 mM EDTA, 1.5 mM Na_3VO_4, 50 mM NaF, 10 mM sodium pyrophosphate, 10 mM sodium β-glycerophosphate, 0.5% Triton X-100, and protease inhibitor tablet [Roche, cat. #11777700]). Protein content was quantified using a Bio-Rad protein assay reagent (Bio-Rad, cat. #500-0006). Equal amounts of protein were resolved on SDS-polyacrylamide gels. Proteins were transferred onto a PVDF membrane, blocked with 5% milk, and incubated with the appropriate primary and secondary antibodies. The membranes were developed with chemiluminescence reagent (5 ml of 100 mM TRIS buffer [pH 8.5] and 5 μl of 30% H_2O_2 were mixed with 10 ml of 100 mM TRIS buffer [pH 8.5], 11 μl of 90 mM p-coumaric acid, and 25 μl of 250 mM luminol and immediately added to the PVDF membrane for 1 min). To test for equivalent loading in each lane, blots were stripped, blocked, and probed with an anti-eIF-4E antibody.

Flow cytometry

RKO, RKO-E6, or HeLa cells were seeded in 20 cm dishes in 10 ml of growth medium. Cells were allowed to adhere and then treated with the selected compounds for 24 hr. The treated cells were collected, washed 2× with

Figure 8. Synthesis of indoxin affinity probes

Synthesis of indoxin probes. Abbreviations: Boc, *t*-butoxycarbonyl; CDI, N,N′-carbonyldiimidazole; DIPEA, diisopropylethylamine; DMF, dimethylformamide; DMSO, dimethyl sulfoxide; Fmoc, 9-fluorenylmethoxycarbonyl; HBTU, *O*-benzotriazol-1-yl-*N*,*N*,*N*′,*N*′-tetramethyluronium hexafluorophosphate; PFP, pentafluorophenol; TFA, trifluoroacetic adic; TFP, tetrafluorophenol.

PBS, and counted. The cell pellet was resuspended in 500 μl of ice-cold PBS, and 2–5 ml of cold 70% ethanol (−20ºC) was added. Cells were fixed for 1 hr or overnight at 4ºC. Five to ten million cells were placed into a 15 ml conical tube and centrifuged at 1000 g. Cells were washed 2× with 1% calf serum in PBS. Cells were resuspended in 800 μl of 1% calf serum in PBS, and 100 μl of RNase (1 mg/ml) and 100 μl of propidium iodide (400 μg/ml) were added. Cells were incubated at 37ºC for 30 min and then analyzed by flow cytometry.

Synthesis of affinity probes

Solvents were purchased from Aldrich and used without further purification. Common synthetic reagents were obtained from commercial sources and used without further purification. Structures are shown in Figure 8 (see legend for abbreviations).

Indoxin derivative I

T13M7 (10 mg, 1 eq.) was dissolved in methylene chloride and added to PFP-biotin (12 mg, 1 eq., Pierce, cat. #21218) solution in DMF. The reaction was stirred for 1 hr at RT and for 30 min at 40ºC. A yield of >95% was confirmed by LC-MS. Solvents and pentafluorophenol were removed under high vacuum, and the crude product was used without further purification.

Indoxin derivative II

BOC-6-aminohexanoic acid (36 mg, 1.1 eq.) was dissolved in chloroform, and CDI (27 mg, 1.2 eq.) was added to the reaction solution. The reaction mixture was stirred at RT for 30 min, and then T13M7 (50 mg, 1 eq.) was added to the reaction. The coupling reaction proceeded slowly and required heating at 50ºC and addition of one more equivalent of CDI. The BOC-protecting group was removed with 30% TFA/70% CH_2Cl_2 at RT for 30 min. Solvents and TFA were removed under high vacuum, and the crude product was extracted with $CHCl_3$/5% K_2CO_3 solution. Organic phase was separated, washed with dH_2O twice, and dried under vacuum to provide the product in Figure 8A. The product (12 mg, 1 eq.) was dissolved in chloroform and added to the PFP-biotin (7 mg, 1 eq.) solution in DMSO, followed by DIPEA (20 μl). The reaction was stirred at RT for 30 min. LC-MS analysis confirmed complete coupling. Chloroform, DIPEA, and pentafluorophenol were removed under high vacuum, and the crude product was used without further purification.

Indoxin derivative III

T13M7 (2.3 mg, 1 eq.) was dissolved in chloroform and added to TFP-PEO-biotin (4.7 mg, 1 eq., Pierce, cat. #21219) solution in chloroform. The reaction was stirred for 1 hr at RT. LC-MS analysis indicated complete consumption of TFP-PEO-biotin, ~75% of product, and ~25% of T13M7 excess. The solvent and tetrafluorophenol were removed under high vacuum; the crude product was triturated with ethyl ether to remove the excess of T13M7 and dried under vacuum. The product was used without further purification.

Benzophenone-biotin V

N-(+)-Biotinyl-6-aminohexanoic acid (239 mg) and 4-benzoyl-L-phenylalanyl-6-aminoxehanoic acid methyl ester (237 mg) were dissolved in DMF, and 230 μl of DIPEA was added to the reaction mixture, followed by 237 mg of HBTU. The reaction mixture was stirred at RT for 30 min. LC-MS analysis showed complete reaction. The solvent and excess of DIPEA were removed under high vacuum. The crude product was dissolved in $CHCl_3$ and extracted 2× with 1% HCl. Organic phase was separated, solvent was removed, and the product was purified using rotary chromatography (SiO_2 solid phase). Yield 325 mg (73.4%).

Indoxin-benzophenone-biotin IV

1. Compound V (100 mg) was dissolved in aqueous methanol, 1 eq. of LiOH was added to the reaction mixture, and the reaction was refluxed overnight. LC-MS analysis confirmed quantitative hydrolysis of the methyl ester. The crude product was dissolved in $CHCl_3$ and extracted with 1% HCl and dH_2O. Organic phase was separated and dried over anhydrous Na_2SO_4 for 1 hr. Then, Na_2SO_4 was filtered off, and solvents were removed under vacuum to provide pure product in a quantitative yield.

2. N-[N-(+)-Biotinyl-6-aminohexanoyl]-4-benzoyl-L-phenylalanyl-6-aminoxehanoic acid (Figure 8C) was dissolved in $CHCl_3$, and 1.1 eq. of CDI was added to the reaction mixture. The reaction was stirred at RT for 30 min, and then T13M7 was added to the reaction. The reaction was stirred at RT for 1 hr and at 50ºC for 30 min. LC-MS analysis confirmed complete coupling. The solution of the crude product in $CHCl_3$ was extracted with 0.1% HCl and dH_2O. The organic phase was separated and dried over anhydrous Na_2SO_4 for 1 hr. Then, Na_2SO_4 was filtered off, and solvents were removed under vacuum to provide more than 90% pure product: indoxin-benzophenone-biotin VI.

Benzophenone-fluorescein VII

1. BOC-6-aminohexanoic acid (105 mg) was dissolved in ~5 ml of $CHCl_3$, and 1.1 eq. of CDI (74 mg) was added to the reaction. The reaction mixture was stirred under argon at RT for 30 min. Then, 180 mg of 4-benzoyl-L-phenylalanyl-6-aminoxehanoic acid methyl ester (Figure 8B) was added to the reaction, and the reaction mixture was stirred at RT for 2 hr. LC-MS analysis indicated complete coupling. The crude product solution in $CHCl_3$ was extracted twice with H_2O (pH ~3) and once with dH_2O to remove imidazole. The organic phase was separated, and the solvent was removed under vacuum. The oily product was dissolved in 3 ml of CH_2Cl_2, and 1 ml of TFA was added to the reaction. The reaction mixture was stirred at RT for 30 min. LC-MS and TLC analysis indicated complete removal of BOC-protecting group, which provided quantitative yield of the compound in Figure 8D.

2. Fifty milligrams of the compound in Figure 8D was dissolved in ~1 ml of DMF and added to the solution of 5-(and-6)-carboxyfluorescein succinimidyl ester (46.5 mg) in DMF. The reaction mixture was stirred at RT for 2 hr and heated at 50ºC for 15 min. Solvents were removed, and the crude product was used for the next step without further purification: the crude product was dissolved in CH_3OH/H_2O (1:1), and LiOH was added to the reaction mixture till pH 11. The reaction was refluxed for 1 hr. LC-MS analysis indicated complete hydrolysis of methyl ester. Then, solvents were removed under vacuum, and the crude product was dissolved in $CHCl_3$/EtOH and extracted with acidic water (pH = 1). The organic phase was separated, and the crude product was purified using rotary TLC (SiO_2 solid phase) to provide benzophenone-fluorescein VII.

Indoxin-benzophenone-fluorescein VI

Benzophenone-fluorescein probe VII (6.8 mg) and T13M7 (2.86 mg) were dissolved in 1 ml of DMF. DIPEA and HBTU (2.8 mg) were added to the reaction mixture, and the reaction mixture was stirred at RT for 30 min. LC-MS analysis indicated only ~50% coupling; therefore, another 2.8 mg of HBTU was added, and the reaction mixture was heated at 50ºC for 10 min. LC-MS analysis confirmed more than 90% coupling reaction. DMF was removed under high vacuum to provide crude product. The oily residue was triturated with Et_2O to remove excess of T13M7, DIPEA, and HBTU byproducts. Then, the product—indoxin-benzophenone-fluorescein VI—was used without further purification.

Affinity purification of protein targets

Biotinylated indoxin probes

RKO-E6 cells were lysed in the nondenaturing lysis buffer (1% NP-40, 50 mM Tris·HCl, pH 7.4, 300 mM NaCl, 5 mM EDTA, 0.02% sodium azide, 10 mM iodoacetamide, 1 mM PMSF, and protease inhibitor tablet [Roche, cat. #11777700]). The cell lysates were precleared with Immobilized NeutrAvidin gel (Pierce Biotechnology, cat. #29200) for 1 hr at 4ºC. Then, the cell lysates were incubated with the small molecule affinity probes for 10–12 hr at 4ºC. NeutrAvidin beads were added to the cell lysates and incubated with the indoxin probes I, II, and III composed of an indoxin moiety, a linker, and biotin. The beads were incubated at 4ºC for 1 hr. Then, the NeutrAvidin beads were separated from the cell lysates and washed twice with the nondenaturing lysis buffer and twice with PBS (for 1D analysis) or with dH_2O (for 2D analysis). The samples for 1D analysis were boiled in SDS page buffer and resolved using Tris-Glycine precast gels. Proteins were detected with Coomassie blue or silver stain. The samples for 2D analysis were sonicated in ZOOM 2D Protein Solubilizer 1 (Invitrogen, cat. #ZS10001) and resolved following the protocol provided by Invitrogen. The cell lysates with the photoreactive probes IV and V were placed in the optical glass cells (Starna, cat. #1-SOG-10-GL14-S), purged with argon gas for 5 min, and irradiated at 350 nm for 15 min in Rayonet Reactor. The crosslinked proteins were isolated and resolved as described above. Western blot analysis was done using anti-biotin antibody.

Fluoresceinylated indoxin probes

The above described protocol was used to isolate proteins crosslinked to photoreactive probes VI and VII using total cell lysates. The nuclear and cytosolic fractions were separated following the published protocol (Lee et al., 1988; Lee and Green, 1990), except the cytoplasmic and the nuclear fractions were used for the affinity purification without dialysis. The affinity purification was done as described above, except that protein A beads and anti-fluorescein antibody were used for the pull-down of crosslinked proteins.

Supplemental data

The Supplemental Data include five supplemental figures, two supplemental Excel files, a zip file containing four SDF files, and a text file explaining the fields in the SDF files. The Supplemental Data can be found with this article online at http://www.cancercell.org/cgi/content/full/9/2/133/DC1/.

Acknowledgments

B.R.S. is supported by a Career Award at the Scientific Interface from the Burroughs Welcome Fund and by the National Cancer Institute (R01 CA097061). M.P. was funded in part by the SURF undergraduate fellowship from the Columbia University. O.B. was in part supported by the UROP undergraduate research fellowship from MIT.

Received: September 16, 2005
Revised: November 21, 2005
Accepted: January 10, 2006
Published: February 13, 2006

References

Asano, T., Nakamura, K., Fujii, H., Horichi, N., Ohmori, T., Hasegawa, K., Isoe, T., Adachi, M., Otake, N., and Fukunaga, Y. (2005). Altered expression of topoisomerase IIα contributes to cross-resistant to etoposide K562/MX2 cell line by aberrant methylation. Br. J. Cancer *92*, 1486–1492.

Beerheide, W., Sim, M.M., Tan, Y.J., Bernard, H.U., and Ting, A.E. (2000). Inactivation of the human papillomavirus-16 E6 oncoprotein by organic disulfides. Bioorg. Med. Chem. *8*, 2549–2560.

Bonner, J.A., and Lawrence, T.S. (1989). Protection of doxorubicin cytotoxicity by cycloheximide. Int. J. Radiat. Oncol. Biol. Phys. *16*, 1209–1212.

Bosch, F.X., Manos, M.M., Munoz, N., Sherman, M., Jansen, A.M., Peto, J., Schiffman, M.H., Moreno, V., Kurman, R., and Shah, K.V. (1995). Prevalence of human papillomavirus in cervical cancer: a worldwide perspective. International biological study on cervical cancer (IBSCC) Study Group. J. Natl. Cancer Inst. *87*, 796–802.

Budihardjo, I.I., Boerner, S.A., Eckdahl, S., Svingen, P.A., Rios, R., Ames, M.M., and Kaufmann, S.H. (2000). Effect of 6-aminonicotinamide and other protein synthesis inhibitors on formation of platinum-DNA adducts and cisplatin sensitivity. Mol. Pharmacol. *57*, 529–538.

Butz, K., Denk, C., Ullmann, A., Scheffner, M., and Hoppe-Seyler, F. (2000). Induction of apoptosis in human papillomaviruspositive cancer cells by peptide aptamers targeting the viral E6 oncoprotein. Proc. Natl. Acad. Sci. USA *97*, 6693–6697.

Butz, K., Ristriani, T., Hengstermann, A., Denk, C., Scheffner, M., and Hoppe-Seyler, F. (2003). siRNA targeting of the viral E6 oncogene efficiently kills human papillomavirus-positive cancer cells. Oncogene *22*, 5938–5945.

Choi, K.H., Choi, H.Y., Ko, J.K., Park, S.S., Kim, Y.N., and Kim, C.W. (2004). Transcriptional regulation of TNF family receptors and Bcl-2 family by chemotherapeutic agents in murine CT26 cells. J. Cell. Biochem. *91*, 410–422.

Chow, K.C., and Ross, W.E. (1987). Topoisomerase-specific drug sensitivity in relation to cell cycle progression. Mol. Cell. Biol. *7*, 3119–3123.

Collot-Teixeira, S., Bass, J., Denis, F., and Ranger-Rogez, S. (2004). Human tumor suppressor p53 and DNA viruses. Rev. Med. Virol. *14*, 301–319.

Dorman, G., and Prestwich, G.D. (1994). Benzophenone photophores in biochemistry. Biochemistry *33*, 5661–5673.

Dorman, G., and Prestwich, G.D. (2000). Using photolabile ligands in drug discovery and development. Trends Biotechnol. *18*, 64–77.

Finzer, P., Kuntzen, C., Soto, U., zur Hausen, H., and Rosl, F. (2001). Inhibitors of histone deacetylase arrest cell cycle and induce apoptosis in cervical carcinoma cells circumventing human papillomavirus oncogene expression. Oncogene *20*, 4768–4776.

Finzer, P., Krueger, A., Stohr, M., Brenner, D., Soto, U., Kuntzen, C., Krammer, P.H., and Rosl, F. (2004). HDAC inhibitors trigger apoptosis in HPV-positive cells by inducing the E2F-p73 pathway. Oncogene *23*, 4807–4817.

Furusawa, S., Nakano, S., Kosaka, K., Takayanagi, M., Takayanagi, Y., and Sasaki, K. (1995). Inhibition of doxorubicin-induced cell death in vitro and in vivo by cycloheximide. Biol. Pharm. Bull. *18*, 1367–1372.

Gastaud, J.M., Senelar, R., and Pujol, H. (1998). C. R. Acad. Sci. III *321*, 5–10.

Hainaut, P., Hernandez, T., Robinson, A., Rodriguez-Tome, P., Flores, T., Hollstein, M., Harris, C.C., and Montesano, R. (1998). IARC Database of p53 gene mutations in human tumors and cell lines: updated compilation, revised formats and new visualisation tools. Nucleic Acids Res. *26*, 205–213.

Hanahan, D., and Weinberg, R.A. (2000). The hallmarks of cancer. Cell *100*, 57–70.

Hermanson, G. (1996). Bioconjugate techniques (San Diego, CA: Academic Press)., pp. 570–591.

Houlbrook, S., Harris, A.L., Carmichael, J., and Stratford, I.J. (1996). Relationship between topoisomerase II levels and resistance to topoisomerase II inhibitors in lung cancer cell lines. Anticancer Res. *16*, 1603–1610.

Johnstone, R.W., Ruefli, A.A., and Lowe, S.W. (2002). Apoptosis: A link between cancer genetics and chemotherapy. Cell *108*, 153–164.

Keith, C.T., Borisy, A.A., and Stockwell, B.R. (2005). Multicomponent therapeutics for networked systems. Nat. Rev. Drug Discov. *4*, 71–78.

Kelley, B.P., Lunn, M.R., Root, D.E., Flaherty, S.P., Martino, A.M., and Stockwell, B.R. (2004). A flexible data analysis tool for chemical genetic screens. Chem. Biol. *11*, 1495–1503.

Kellner, U., Sehested, M., Jensen, P.B., Gieseler, F., and Rudolph, P. (2002). Culprit and victim-DNA topoisomerase II. Lancet Oncol. *3*, 235–243.

Koshiyama, M., Fujii, H., Kinezaki, M., Morita, Y., Nanno, H., and Yoshida, M. (2001). Immunohistochemical expression of topoisomerase IIα (Topo IIα) and multidrug resistance-associated protein (MRP), plus chemosensitivity testing, as chemotherapeutic indices of ovarian and endometrial carcinomas. Anticancer Res. *21*, 2925–2932.

Krishna, R., and Mayer, L.D. (2000). Multidrug resistance (MDR) in cancer. Mechanisms, reversal using modulators of MDR and the role of MDR modulators in influencing the pharmacokinetics of anticancer drugs. Eur. J. Pharm. Sci. *11*, 265–283.

Larsen, A.K., and Skladanowski, A. (1998). Cellular resistance to topoisomerase-targeted drugs: from drug uptake to cell death. Biochim. Biophys. Acta *1400*, 257–274.

Lee, K.A., and Green, M.R. (1990). Small-scale preparation of extracts from radiolabeled cells efficient in pre-mRNA splicing. Methods Enzymol. *181*, 20–30.

Lee, K.A., Bindereif, A., and Green, M.R. (1988). A small-scale procedure for preparation of nuclear extracts that support efficient transcription and pre-mRNA splicing. Gene Anal. Tech. *5*, 22–31.

Levine, A.J. (1997). p53, the cellular gatekeeper for growth and division. Cell *88*, 323–331.

Lunn, M.R., Root, D.E., Martino, A.M., Flaherty, S.P., Kelley, B.P., Coovert, D.D., Burghes, A.H., Man, N.T., Morris, G.E., Zhou, J., et al. (2004). Indoprofen upregulates the survival motor neuron protein through a cyclooxygenase-independent mechanism. Chem. Biol. *11*, 1489–1493.

MacGrogan, G., Rudolph, P., Mascarel Id, I., Mauriac, L., Durand, M., Avril, A., Dilhuydy, J.M., Robert, J., Mathoulin-Pelissier, S., Picot, V., et al. (2003). DNA topoisomerase IIα expression and the response toprimary chemotherapy in breast cancer. Br. J. Cancer *89*, 666–671.

Maehama, T., Patzelt, A., Lengert, M., Hutter, K.J., Kanazawa, K., Hausen, H., and Rosl, F. (1998). Selective down-regulation of human papillomavirus transcription by 2-deoxyglucose. Int. J. Cancer *76*, 639–646.

Michael, D., and Oren, M. (2003). The p53-Mdm2 module and the ubiquitin system. Semin. Cancer Biol. *13*, 49–58.

Munger, K., Phelps, W.C., Bubb, V., Howley, P.M., and Schlegel, R. (1989). The E6 and E7 genes of the human papillomavirus type 16 together are

necessary and sufficient for transformation of primary human keratinocytes. J. Virol. *63*, 4417–4421.

Nociari, M.M., Shalev, A., Benias, P., and Russo, C. (1998). A novel one-step, highly sensitive fluorometric assay to evaluate cell-mediated cytotoxicity. J. Immunol. Methods *213*, 157–167.

Olivier, M., Eeles, R., Hollstein, M., Khan, M.A., Harris, C.C., and Hainaut, P. (2002). The IARC TP53 database: new online mutation analysis and recommendations to users. Hum. Mutat. *19*, 607–614.

Patarca, R., and Fletcher, M.A. (1995). Effects of benzalkonium salts on eukaryotic and microbial G-protein-mediated processes and surface membranes. Crit. Rev. Oncog. *6*, 327–356.

Patarca, R., Rosenzwei, J.A., Zuniga, A.A., and Fletcher, M.A. (2000). Benzalkonium salts: effects on G protein-mediated processes and surface membranes. Crit. Rev. Oncog. *11*, 255–305.

Pestic-Dragovich, L., Stojiljkovic, L., Philimonenko, A.A., Nowak, G., Ke, Y., Settlage, R.E., Shabanowitz, J., Hunt, D.F., Hozak, P., and de Lanerolle, P. (2000). A myosin I isoform in the nucleus. Science *290*, 337–341.

Prestwich, G.D., Dorman, G., Elliott, J.T., Marecak, D.M., and Chaudhary, A. (1997). Benzophenone photoprobes for phosphoinositides, peptides and drugs. Photochem. Photobiol. *65*, 222–234.

Root, D.E., Flaherty, S.P., Kelley, B.P., and Stockwell, B.R. (2003). Biological mechanism profiling using an annotated compound library. Chem. Biol. *10*, 881–892.

Rosl, F., Das, B.C., Lengert, M., Geletneky, K., and zur Hausen, H. (1997). Antioxidant-induced changes of the AP-1 transcription complex are paralleled by a selective suppression of human papillomavirus transcription. J. Virol. *71*, 362–370.

Scheffner, M., Werness, B.A., Huibregtse, J.M., Levine, A.J., and Howley, P.M. (1990). The E6 oncoprotein encoded by human papillomavirus types 16 and 18 promotes the degradation of p53. Cell *63*, 1129–1136.

Scheffner, M., Huibregtse, J.M., Vierstra, R.D., and Howley, P.M. (1993). The HPV-16 E6 and E6-AP complex functions as a ubiquitin-protein ligase in the ubiquitination of p53. Cell *75*, 495–505.

Schiffman, M.H., and Castle, P. (2003). Epidemiologic studies of a necessary causal risk factor: human papillomavirus infection and cervical neoplasia. J. Natl. Cancer Inst. *95*, E2.

Slebos, R.J., Kessis, T.D., Chen, A.W., Han, S.M., Hedrick, L., and Cho, K.R. (1995). Functional consequences of directed mutations in human papillomavirus E6 proteins: abrogation of p53-mediated cell cycle arrest correlates with p53 binding and degradation in vitro. Virology *208*, 111–120.

Smukste, I., and Stockwell, B.R. (2005). Advances in chemical genetics. Annu. Rev. Genomics Hum. Genet. *6*, 261–286.

Stockwell, B.R. (2000a). Chemical genetics: ligand-based discovery of gene function. Nat. Rev. Genet. *1*, 116–125.

Stockwell, B.R. (2000b). Frontiers in chemical genetics. Trends Biotechnol. *18*, 449–455.

Stockwell, B.R. (2004). Exploring biology with small organic molecules. Nature *432*, 846–854.

Thomas, M., and Banks, L. (1998). Inhibition of Bak-induced apoptosis by HPV-18 E6. Oncogene *17*, 2943–2954.

Veldman, T., Horikawa, I., Barrett, J.C., and Schlegel, R. (2001). Transcriptional activation of the telomerase hTERT gene by human papillomavirus type 16 E6 oncoprotein. J. Virol. *75*, 4467–4472.

von Knebel Doeberitz, M., Rittmuller, C., zur Hausen, H., and Durst, M. (1992). Inhibition of tumorigenicity of cervical cancer cells in nude mice by HPV E6-E7 anti-sense RNA. Int. J. Cancer *51*, 831–834.

Weber, P.J., and Beck-Sickinger, A.G. (1997). Comparison of the photochemical behavior of four different photoactivatable probes. J. Pept. Res. *49*, 375–383.

zur Hausen, H. (1996). Papillomavirus infections—a major cause of human cancers. Biochim. Biophys. Acta *1288*, F55–F78.

zur Hausen, H. (2000). Papillomaviruses causing cancer: evasion from host-cell control in early events in carcinogenesis. J. Natl. Cancer Inst. *92*, 690–698.

zur Hausen, H. (2002). Papillomaviruses and cancer: from basic studies to clinical application. Nat. Rev. Cancer *2*, 342–350.